ACS NANO

www.acsnano.org

ARTICLE

Large Exciton Polaron Formation in 2D Hybrid Perovskites via Time-Resolved Photoluminescence

Sebastian Hurtado Parra, Daniel B. Straus, Bryan T. Fichera, Natasha Iotov, Cherie R. Kagan, and James M. Kikkawa*

Cite This: *ACS Nano* 2022, 16, 21259–21265

Read Online

ACCESS | Metrics & More | Article Recommendations | Supporting Information

ABSTRACT: **We find evidence for the formation and relaxation of large exciton polarons in 2D organic–inorganic hybrid perovskites. Using ps-scale time-resolved photoluminescence within the phenethylammonium lead iodide family of compounds, we identify a red shifting of emission that we associate with exciton polaron formation time scales of 3–10 ps. Atomic substitutions of the phenethylammonium cation allow local control over the structure of the inorganic lattice, and we show that the structural differences among materials strongly influence the exciton polaron relaxation process, revealing a polaron binding energy that grows larger (up to 15 meV) in more strongly distorted compounds.**

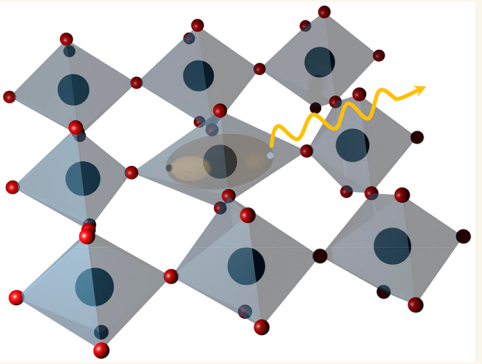

KEYWORDS: *2D perovskites, time-resolved photoluminescence, transient PL, transient absorption, exciton polarons, octahedral distortions*

Hybrid organic–inorganic perovskites continue to be at the forefront of materials science research due to their potential for efficient and cheaply manufacturable photovoltaics and light-emitting diodes.[1] These materials can be three-dimensional hybrid perovskites (3DHPs) in bulk or nanocrystalline form, composed of metal-halide octahedra and small inorganic or organic cations, or two-dimensional hybrid perovskites (2DHPs), in which sheets of metal-halide octahedra are spaced by interposed larger organic cationic layers.[2] A key attribute of this material family is a strong electron- and exciton–phonon coupling.[3,4] In 3DHPs, charge introduced via electrical injection or photogeneration and separation is hypothesized to evolve into charged lattice polarons with defect-tolerant transport properties.[5,6] Pulsed laser experiments can stimulate and witness the formation and relaxation of polaronic complexes, but contrasting results have been obtained depending on the type of probe used. Studies using time-delayed optical probes of electronic dynamics have inferred subpicosecond charge polaron formation in bulk[7−11] and nanocrystalline[12] 3DHPs. In contrast, diffractive electron or X-ray probes show structural relaxation on much longer relaxation time scales, up to 10 ps.[13,14] Additional studies are therefore desirable to clarify the relationship between electronic and structural dynamics in hybrid perovskites.

In 2DHPs, exciton–phonon coupling under optical excitation is more relevant because quantum and dielectric confinement effects yield large >100 meV exciton binding energies. In the most commonly studied 2DHPs, band edge states in these materials originate from the inorganic sublattice,[15,16] which leads to an effectively two-dimensional (2D) electronic system. The optical spectra of 2DHPs are dominated by excitonic states with binding energies in excess of 100 meV,[17] allowing detailed study of the exciton–phonon coupling by monitoring the excitonic resonance.[18] Impulsively simulated coherent phonons appearing in time-resolved absorption (TRA) arise on subpicosecond time scales and identify Raman active modes which are likely to participate in exciton polaron formation.[19] However, the evolution of the exciton into an exciton polaron through quasi-static reconfiguration of the lattice does not appear in this method, and structural responses to photoexcitation recorded by electron

Received: September 16, 2022
Accepted: December 9, 2022
Published: December 15, 2022

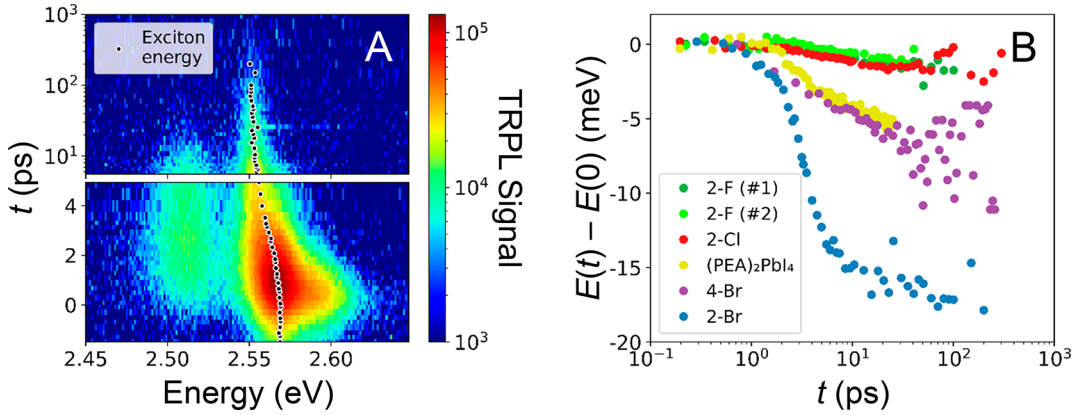

Figure 1. (A) 12K TRPL map for 2-Br. Black dots indicate the energy position of the central exciton resonance. (B) Temporal energy shift of the central exciton for the studied compounds (data collected between 10 and 15 K).

diffraction in 2DHPs show the experimental time scale for quasi-static, nonoscillatory lattice reorganization is ∼10 ps.[20]

Here, we report the formation of large, uncharged *exciton* polarons in 2D hybrid perovskites (2DHPs) coupled to quasi-static lattice distortions. Using time-resolved photoluminescence (TRPL), we uncover a spectral red shift of the central exciton emission that evolves over coincident 10 ps time scales. Additional juxtaposition of TRPL dynamics with TRA and time-integrated optical spectra suggests that the red shift signals the formation and evolution of a large exciton polaron, with a binding energy that grows larger in more strongly distorted compounds. Our work directly reveals the formation of large exciton polaron complexes in 2DHPs and highlights their relevance to recent measurements of structural dynamics in 2DHPs.[20]

RESULTS AND DISCUSSION

Our samples are 2DHPs in the phenethylammonium (PEA) lead iodide family where a single atom on the cation is replaced with a larger and heavier atom. $(PEA)_2PbI_4$ is a prototypical 2DHP for which two classes of excitons are most commonly discussed: self-trapped excitons (STEs) with large Stokes shifts (∼300 meV) and broad emission profiles (>100 meV line widths),[21] and free Wannier excitons exhibiting much smaller Stokes shifts (∼10 meV) and sharp absorption/emission line widths (∼10 meV).[18] STEs are believed to originate from self-trapped, small polaron states that arise due to strong exciton−phonon coupling. Wannier excitons also show signs of exciton−phonon scattering,[22] and low temperature spectra exhibit fine structure which has been attributed to vibrational sidebands[23] or distinct excitons showing strong polaronic coupling.[24]

We prepare $(PEA)_2PbI_4$ as well as derivatives that incorporate 2- and 4-position (*ortho* and *para*) substitutions of a hydrogen atom on the phenyl moiety of the cation with a halogen: $(2\text{-FPEA})_2PbI_4$, $(2\text{-ClPEA})_2PbI_4$, $(2\text{-BrPEA})_2PbI_4$, and $(4\text{-BrPEA})_2PbI_4$, which we abbreviate as 2-F, 2-Cl, 2-Br, and 4-Br. The structural characteristics of these compounds have been explored in previous work through single crystal X-ray diffraction measurements.[25,26] 4-site substitutions lengthen the interlayer distance between inorganic sheets, but do not otherwise change the structure of the inorganic lattice significantly as measured by the average in-plane Pb−I−Pb bond angle and Pb−I bond length. In contrast, 2-site substitutions increase the cross-sectional area of the organic cation, inducing distortions of the in-plane Pb−I−Pb bond angle relative to the unsubstituted PEA compound. In the strongest case of distortion (2-Br), there is an additional out-of-plane buckling of the inorganic structure that is not present in $(PEA)_2PbI_4$, 2-F, 2-Cl, or 4-Br.[27] For transient spectroscopy, we measure thin films that are spin-cast from perovskite crystals dissolved in acetonitrile (for $(PEA)_2PbI_4$, 2-F, 2-Cl and 2-Br), or dimethylformamide (for 4-Br).

The TRPL measurements presented here expand those published previously,[23,26] focusing on signatures of polaron formation, and are performed inside of a cryostat held at a constant temperature in the range of 10−15 K using an optical Kerr gate configuration described in our earlier work.[23,26] Briefly, we exploit the transient birefringence induced by an intense laser pulse (optical Kerr effect) in CS_2 as an ultrafast optical gate for the sample PL generated by a second pump pulse. The PL can then be time-resolved by varying the relative time delay between the two laser pulses. The setup has the advantages of subpicosecond temporal resolution and broadband spectral detection, which allow for the observation of the TRPL shifts discussed in this work. The results are PL spectra at various pump−probe delays as visualized in the 2D TRPL maps of Figure 1A and S1. We fit the spectrum at each delay to a sum of multiple Gaussians, and extract the energy of the central excitonic resonance vs time, indicated by the black points in Figure 1A. The energy of the central exciton red shifts over time for all of the measured compounds. To enable a comparison of red shifts between different compounds, we plot the central exciton energy shift induced by the pump pulse relative to zero delay (Figure 1B). Note that for the compound 2-F we consider two distinct exciton states.[26] Figure 1B shows that the TRPL red shifts occur over 10 ps and reveals that the magnitude of the red shift is smallest for 2-F and 2-Cl, intermediate for PEA and 4-Br, and largest for 2-Br. In the following we will argue that the TRPL red shift for 2-Br, and quite possibly for all compounds, represents the relaxation of an exciton polaron minimizing its energy as it distorts the surrounding lattice.

To explore a potential polaronic origin of the TRPL red shift, we first look for a connection with lattice distortion. The degree of intraoctahedral lattice distortion for the inorganic Pb−I octahedra can be quantified by the bond angle variance[28] σ^2:

https://doi.org/10.1021/acsnano.2c09256
ACS Nano 2022, 16, 21259−21265

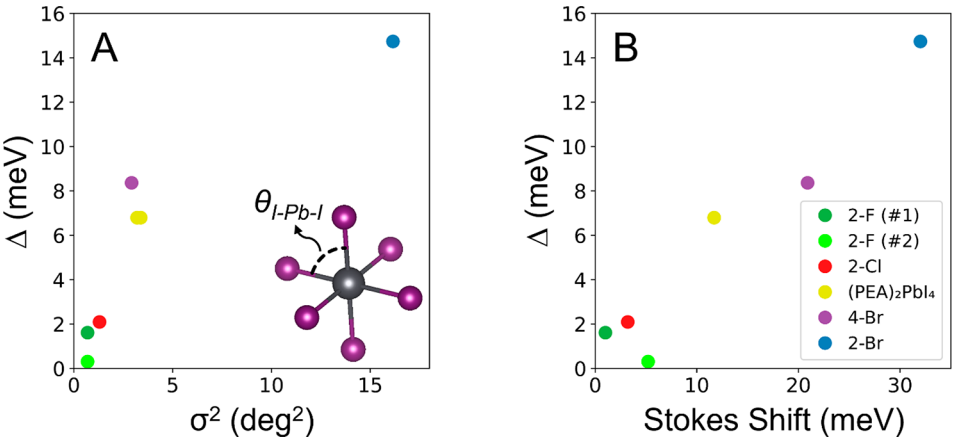

Figure 2. (A) TRPL red shift magnitude Δ versus bond angle variance σ^2 (defined in the main text) and (B) TRPL red shift magnitude Δ versus the steady-state Stokes shift of the central exciton transition (defined as the energy difference between the central excitonic absorption and PL resonances). TRPL data collected between 10 and 15 K, and all the structural parameters are taken from 100 K crystal structures.

$$\sigma^2 = \sum_{i}^{12} (\theta_i - 90°)^2/11$$

where θ_i is the I−Pb−I angle for adjacent octahedral vertices as measured by single-crystal X-ray diffraction (SCXRD).[25,26] Figure 2A shows a strong correlation between the magnitude of the TRPL red shift (Δ, obtained from the *y*-axis intercept of the data in Figure S3) and σ^2 for each compound, indicating that more strongly distorted octahedra increase the exciton energy shift (a similar analysis for interoctahedral distortion yielded no correlation). This trend supports an exciton polaron picture, as more distorted lattices have shown stronger structural changes upon photoexcitation[20,29] for 3DHPs and 2DHPs. We note that interoctahedral distortion plays a primary role in the formation of smaller, self-trapped excitons in 2DHPs with considerably larger binding energies.[30−34,21]

The TRPL red shift ultimately leads to a Stokes shift in the steady state spectra, which could capture the energy relaxation of the free exciton seen in absorption as it binds into an exciton polaron. Figure 2B shows a plot of the magnitude of the TRPL red shift versus the Stokes shift of the central transition, showing a strong correlation among all compounds. We further note the Stokes shift appears to have additional contributions beyond our estimate (Δ) of the binding energy of the exciton polaron, such as slow energy redistribution in a statically disordered energy landscape.

We quantify the time scale of the energy red shift on a log−linear plot of the peak energy versus time (Figure S3), and find a time constant of 3−10 ps for the initial red shift. For PEA, 4-Br, and 2-Br, a double exponential decay occurs with a secondary red shift time constant of ∼20 ps (Figure S3). These time scales are similar to those associated with lattice relaxation subsequent to optical excitation in 2DHPs.[20] Time-resolved electron scattering measurements in n = 2,3 Dion-Jacobson (DJ) and n = 2,4 Ruddlesden−Popper (RP) phases of 2DHPs (n = number of octahedral metal-halide layers per confining cationic layer) have probed electronically induced relaxation of the Pb−I lattice using transient amplitude changes of the Bragg X-ray diffraction peaks.[20] The dynamics for each diffraction peak were fit to a single exponential to obtain a range of time constants, which are 1 ps −5 ps for DJ phases and 2 ps −15 ps for RP phases. These compounds are not identical to those studied here (our samples are the n = 1, 2D limit), but the observation of structural time scales coinciding with our TRPL red shift dynamics within the same family of compounds further supports exciton polaron formation as responsible for the observed red shift.

Before discussing our hypothesis further, we address alternative explanations for the observed TRPL red shift. First, a temporal red shift in the TRPL could originate from excitons relaxing through a statically disordered energy landscape, as would be caused by diffusion toward intrinsic energetic minima due to localized traps or defects.[35,36] However, the behavior of time-integrated PL measurements from ∼15 to 300 K are inconsistent with a static disorder origin. Figure 3 shows the emission energy of the central PL peak (after subtracting the temperature dependence of the bandgap energy), δE_{PL}, versus the thermal energy, k_BT. The subtracted bandgap energy is obtained from fits of the linear temperature dependence of the absorption energy[25,26] and accounts for any electronic effects due to thermal expansion. If the TRPL shift were due to static disorder, then the

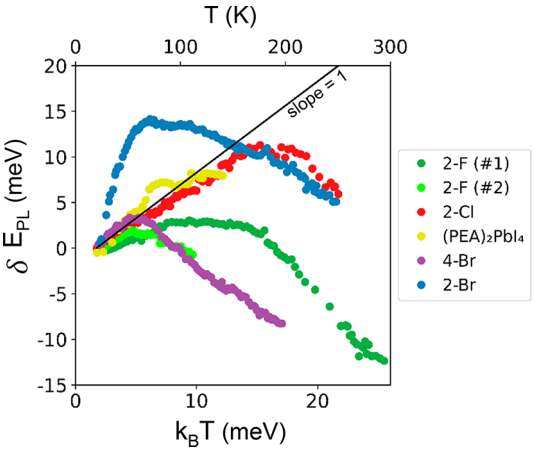

Figure 3. Change of central excitonic PL energy (δE_{PL}) vs thermal energy (k_BT). To compute δE_{PL}, contributions to the PL shift due to changes in the bandgap are subtracted based off a linear fit of the absorption energy versus temperature.

https://doi.org/10.1021/acsnano.2c09256
ACS Nano 2022, 16, 21259−21265

temperature-dependent PL would exhibit thermally assisted activation among a distribution of states and, consequently, the PL of the exciton would blue shift with increasing temperature by *at most* the thermal energy. Figure 3 shows that for 2-Br there is a PL blue shift in excess of the thermal energy indicated by the line of slope unity. The existence of the excess energy shift implicates some other relaxation mechanism besides a static energy landscape, and the correlation with the TRPL shift (Δ, Figure 2) suggests a common origin to these two shifts.

Next, we address the scenario in which TRPL red shifts arise from slow thermalization of the electronic system. In that case, the TRPL line shape would exhibit an asymmetry in the form of a high energy tail due to hot exciton emission, which diminishes over time as the excitons cool. Figures 4A and 4B

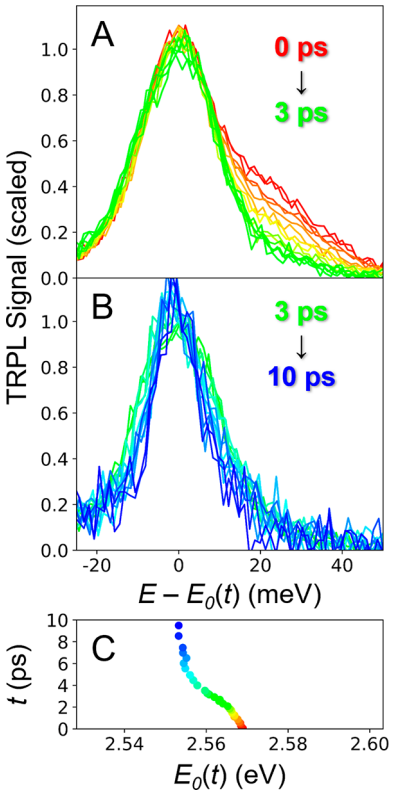

Figure 4. 2-Br TRPL line shape between (A) 0 to 3 ps, and (B) 3 to 10 ps with the time-dependent energy of the central peak, E_0, shown in (C), subtracted. Note that the energy spanned in (C) matches that in (A) and (B) for easy comparison. TRPL data collected at 12 K.

show the temporal evolution of the TPRL spectral line shape of 2-Br. The spectra are normalized and plotted with the center of the peak at 0 meV to facilitate the direct comparison of the time-dependent line shapes. Figure 4C shows the red shift of the central exciton line shape vs time. The plots in Figure 4 share the same energy range, and the energy axis of Figure 4C is set so that the t = 10 ps point coincides with x = 0 meV in Figures 4A and 4B. Similar plots for the rest of the compounds can be found in Figure S2. Although early time data (<3 ps) in Figure 4A shows evidence of thermalization and the disappearance of a high energy tail, subsequent spectra (Figure 4B) show the later line shape remains symmetrical while the peak energy continues to red shift significantly (Figure 4C), demonstrating that the TRPL red shift is not explained by slowed thermalization.

Lastly, many-body effects such as bandgap renormalization and biexciton formation can induce shifts in the energy of excitonic states, which could be observed as a TRPL red shift. However, these are both fast processes in perovskites which occur over subpicosecond time scales,[37−40] unlike the much longer time scales of our TRPL red shift. Energy shifts of the exciton due to many-body effects can be observed in TRA spectra.[41] We measured the TRA of 2-Br (Figure 5A) and extracted the energy of the central resonance. Figure 5B compares the spectral shift in TRA and TRPL and reveals that the TRPL red shift occurs over a longer time scale and is of a larger magnitude than the TRA shift. The excess time and energy of the TRPL shift demonstrates that many-body effects alone cannot adequately account for the observed shift in TRPL.

Having ruled out alternative explanations, we conclude that our data support a scenario of progressive energy minimization of an exciton polaron during its formation. Because the exciton polaron remains emissive during its formation, TPRL provides a direct view of the relaxing electronic complex. Complementary, ultrafast diffraction measurements of structure can map the associated nonthermal deformation of the lattice, but are not yet available for these specific materials. In 3DHP formamidinium lead bromide nanocrystals, pulsed above-gap optical excitation leads to a photoinduced reduction of octahedral tilting (increased Pb−Br−Pb bond angles) compared to the equilibrium structure, as recorded by ultrafast electron diffraction (UED).[29] As the lattice symmetry increases and Pb-X-Pb bond angles approach 180 deg (X = halide atom), greater overlap of adjacent orbitals results in an increase in the conduction and valence bandwidths and a decrease in the bandgap. The presence of excitons thus drives the inorganic framework system toward a more symmetrical square lattice with a smaller bandgap to reduce the exciton energy.[29] We note that in *bulk* 3DHPs, where excitons play a much smaller role because of their greatly reduced binding energy, photoinduced *dis*ordering of the lattice has been reported.[13]

Moving to 2DHPs, another recent exciton study using UED measured an in-plane regularization of the octahedral sublattice,[20] similar to what was observed for formamidinium lead bromide nanocrystals. According to these trends, more distorted 2DHPs should yield larger exciton polaron binding energies, seemingly in agreement with our observations and Figure 2A. An intriguing difference, however, is that the bond angle variance we computed reflects intraoctahedral distortion, whereas octahedral tilting is an interoctahedral distortion. Further studies are required to understand to what extent one can generalize such differences and to establish the lattice changes in the materials studied here. We add that 2-Br, which has the largest TRPL red shift, has a corrugated inorganic structure[26] that accounts for its large bond angle variance and may play an additional role in promoting exciton polaron formation.

Coherent phonon oscillations reported in TRA give an indication of the lattice modes that may be relevant to exciton polaron formation.[42] The sudden appearance of excitons impulsively launches coherent phonons which propagate away from the exciton and modify, through the electron−phonon coupling, the exciton absorption transitions elsewhere in the crystal. The types of phonons generated show how the exciton

https://doi.org/10.1021/acsnano.2c09256
ACS Nano 2022, 16, 21259−21265

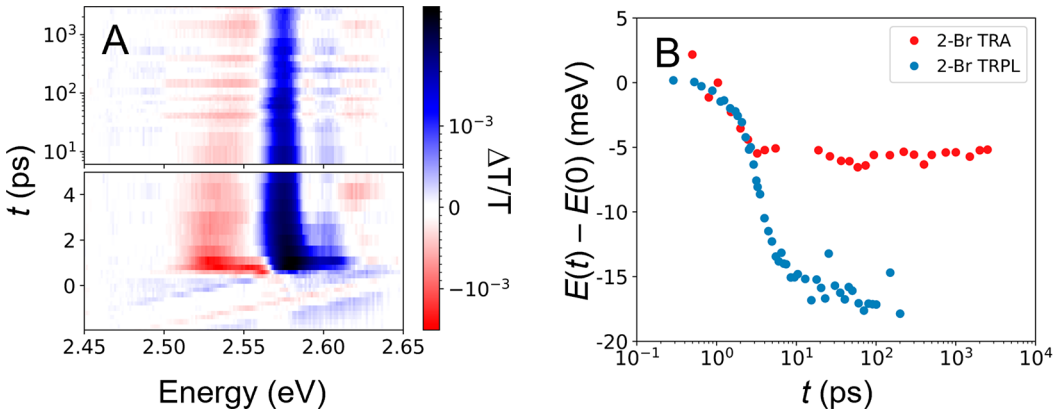

Figure 5. 2-Br (A) TRA map at 12 K and (B) TRPL and TRA exciton energy shifts vs time (both collected at 12 K). The TRA feature is a photobleach of the central excitonic transition.

"tugs" on the lattice, and a superposition of those normal modes can, with proper phase information and knowledge of all exciton−phonon coupling strengths, in principle be used to inform the lattice deformation that initiates exciton polaron formation (assuming all relevant modes are Raman active and of frequencies that may be captured). The majority of the coherent phonon modes identified using TRA affect the interoctahedral (Pb−I−Pb) and intraoctahedral (I−Pb−I) angles,[42] suggesting that octahedral distortions play a strong role in polaron binding.

Tracking the lattice deformation *within* the exciton polaron is a rather different challenge. As long as phonon oscillations are observed in TRA, they cannot report the final lattice configuration, but rather report oscillations about equilibrium. Furthermore, due to phase space considerations, coherent phonon oscillations of the ground state-to-exciton transition preferentially measure lattice vibrations that have propagated *away* from the photoexcited excitons (to locations where the electronic ground state is available). The extent to which the equilibrium lattice coordinates have evolved due to the formation of an exciton polaron is therefore not reflected in TRA of the ground state-to-exciton transition, although such evolution might be inferred through careful analysis of exciton-to-multiexciton transitions. It is further important to highlight that the subpicosecond launch time for coherent phonons does not represent the formation time of a fully formed exciton-polaron complex. Thus, ultrafast direct structural probes such as UED and ultrafast X-ray diffraction are likely to be most effective in revealing the lattice changes accompanying the exciton red shift.

The 1−15 meV magnitude of Δ seen in our measurements needs to be distinguished from the white light emission associated with self-trapped excitons, which correspond to small polarons with radii comparable to the corner-to-corner octahedral distance ($d \sim 0.6$ nm[25,26]) and exhibit much larger Stokes shifts. Here we propose that our measurements instead capture large exciton polarons. Considerable work has been devoted toward studying the *charged* polaron binding energy in both 3D and 2D systems, consisting of a single charge bound to a polaronic cloud.[43−47] Although not directly applicable to *exciton* polarons, the prediction of the charged polaron radius is informative to consider because charged polarons may be regarded as the starting point for exciton formation in these materials, rather than free electrons and holes. Working from studies[43,44] of the Pekar model in 2D, one obtains (see Supporting Information) the following expression relating the charged polaron binding energy, E_b, to polaron radius, r_p in the strong coupling limit: $E_b = \frac{1}{4}\sqrt{\frac{\pi}{2}}\frac{ke^2}{\kappa r_p}$, where k is the Coulomb constant, $\frac{1}{\kappa} = \frac{1}{\varepsilon} - \frac{1}{\varepsilon_0}$, and ε and ε_0 are the dielectric constants at the optical phonon frequency and zero frequency, respectively. Using this model for 2-Br, taking $\kappa = 6$,[48] and dividing the 15 meV binding energy equally between the electron and hole, one obtains a polaron radius of $r_p \sim 10$ nm. Again, a theory for exciton polarons is needed and this estimate for charged polarons is only used here to suggest that consideration of large polarons, $r_p \gg d$, is appropriate. Despite length scale differences between large and small polarons, both show a dependence on lattice distortion, with the small polarons being more common among lattices with strong interoctahedral distortion,[49] and our large polarons showing a correlation between intraoctahedral distortion and binding energy. However, unlike many small polarons whose formation is thought to occur via tunneling through a potential energy barrier,[33,50] the smooth TRPL shift observed here suggests a barrier-less formation and relaxation for the polarons reported here.

CONCLUSIONS

In this paper, we present evidence for the formation of exciton polarons over ∼10 ps following photoexcitation in 2DHPs, as measured by TRPL. The magnitude of the associated red shift is correlated with octahedral distortion in the equilibrium structure and emerges on a time scale that matches structural response time scales directly measured within the 2DHP family.[13,14] Our work mirrors the use of TRPL four decades ago to witness the formation of exciton magnetic polarons in dilute magnetic semiconductors,[51] and moving forward our methods will find synergy with transient structural probes that can clarify the progression of structural distortion accompanying exciton polaron formation.

METHODS

Details about perovskite synthesis and film deposition are found in previous publications.[23,25,26] Samples are held in an Oxford Instruments Microstat crysostat in a vacuum of at least 10^{-4} Torr during optical spectroscopy measurements. Samples are cooled by a continuous flow of liquid helium and a cold finger heat exchanger. The output from a 1 kHz, 800 nm, 120 fs Spectra-Physics Spitfire regenerative amplifier is frequency doubled to 400 nm and focused

https://doi.org/10.1021/acsnano.2c09256
ACS Nano 2022, 16, 21259−21265

onto a 300 μm spot to photoexcite the sample. Excitation power ranges between 1−2 μW for the different samples. TRPL is measured using an optical Kerr gate described previously.[23] For TRA, we tightly focus part of the regenerative amplifier output onto a sapphire plate to produce a supercontinuum probe pulse and measure the transmission of the supercontinuum with and without photoexcitation by the 400 nm pump pulse. Optical spectra are collected using a 0.55 m Jobin-Yvon Triax spectrometer and a Princeton Instruments Spec-10 CCD camera, with a 0.25 nm spectral resolution.

ASSOCIATED CONTENT

Supporting Information

The Supporting Information is available free of charge at https://pubs.acs.org/doi/10.1021/acsnano.2c09256.

Estimate of charged polaron radius, TRPL maps for compounds not shown in the main text, evolution of the TRPL line shape for all compounds, decays of $E(t) - E_{final}$ used estimate the time scale of the TRPL redshift (PDF)

AUTHOR INFORMATION

Corresponding Author

James M. Kikkawa − *Departments of Physics and Astronomy, University of Pennsylvania, Philadelphia, Pennsylvania 19104, USA;* orcid.org/0000-0002-5948-3233; Email: kikkawa@physics.upenn.edu

Authors

Sebastian Hurtado Parra − *Departments of Physics and Astronomy, University of Pennsylvania, Philadelphia, Pennsylvania 19104, USA*

Daniel B. Straus − *Chemistry, University of Pennsylvania, Philadelphia, Pennsylvania 19104, USA;* Present Address: D.B.S.: Department of Chemistry, Princeton University, Princeton, NJ 08544; orcid.org/0000-0003-2977-5590

Bryan T. Fichera − *Departments of Physics and Astronomy, University of Pennsylvania, Philadelphia, Pennsylvania 19104, USA;* Present Address: B.T.F.: Department of Physics, Massachusetts Institute of Technology, Cambridge, MA 02139; orcid.org/0000-0003-1888-7095

Natasha Iotov − *Departments of Physics and Astronomy, University of Pennsylvania, Philadelphia, Pennsylvania 19104, USA;* Present Address: N.I.: Thorlabs, Newton, NJ 07860

Cherie R. Kagan − *Electrical and Systems Engineering, Chemistry, and Materials Science and Engineering, University of Pennsylvania, Philadelphia, Pennsylvania 19104, USA;* orcid.org/0000-0001-6540-2009

Complete contact information is available at: https://pubs.acs.org/10.1021/acsnano.2c09256

Notes

The authors declare no competing financial interest.

ACKNOWLEDGMENTS

S.H.P. and J.M.K. acknowledge support from MRSEC NSF DMR-1720530. D.B.S. acknowledges the National Science Foundation Graduate Research Fellowship under grant DGE-1321851. C.R.K. acknowledges support from the Stephen J. Angello Professorship.

REFERENCES

(1) Green, M. A.; Ho-Baillie, A.; Snaith, H. J. The Emergence of Perovskite Solar Cells. *Nat. Photonics* **2014**, *8*, 506−514.

(2) Mao, L.; Stoumpos, C. C.; Kanatzidis, M. G. Two-Dimensional Hybrid Halide Perovskites: Principles and Promises. *J. Am. Chem. Soc.* **2019**, *141*, 1171−1190.

(3) Wright, A. D.; Verdi, C.; Milot, R. L.; Eperon, G. E.; Perez-Osorio, M. A.; Snaith, H. J.; Giustino, F.; Johnston, M. B.; Herz, L. M. Electron-Phonon Coupling in Hybrid Lead Halide Perovskites. *Nat. Commun.* **2016**, *7*, 11755.

(4) Herz, L. M. How Lattice Dynamics Moderate the Electronic Properties of Metal-Halide Perovskites. *J. Phys. Chem. Lett.* **2018**, *9*, 6853−6863.

(5) Zhu, X.-Y.; Podzorov, V. Charge Carriers in Hybrid Organic−Inorganic Lead Halide Perovskites Might Be Protected as Large Polarons. *J. Phys. Chem. Lett.* **2015**, *6*, 4758−4761.

(6) Zhu, H.; Miyata, K.; Fu, Y.; Wang, J.; Joshi, P. P.; Niesner, D.; Williams, K. W.; Jin, S.; Zhu, X.-Y. Screening in Crystalline Liquids Protects Energetic Carriers in Hybrid Perovskites. *Science* **2016**, *353*, 1409−1413.

(7) Miyata, K.; Meggiolaro, D.; Trinh, M. T.; Joshi, P. P.; Mosconi, E.; Jones, S. C.; De Angelis, F.; Zhu, X.-Y. Large Polarons in Lead Halide Perovskites. *Science Advances* **2017**, *3*, e1701217.

(8) Munson, K. T.; Swartzfager, J. R.; Gan, J.; Asbury, J. B. Does Dipolar Motion of Organic Cations Affect Polaron Dynamics and Bimolecular Recombination in Halide Perovskites? *J. Phys. Chem. Lett.* **2020**, *11*, 3166−3172.

(9) Evans, T. J. S.; Miyata, K.; Joshi, P. P.; Maehrlein, S.; Liu, F.; Zhu, X.-Y. Competition Between Hot-Electron Cooling and Large Polaron Screening in CsPbBr3 Perovskite Single Crystals. *J. Phys. Chem. C* **2018**, *122*, 13724−13730.

(10) Frost, J. M.; Whalley, L. D.; Walsh, A. Slow Cooling of Hot Polarons in Halide Perovskite Solar Cells. *ACS Energy Letters* **2017**, *2*, 2647−2652.

(11) Bretschneider, S. A.; Ivanov, I.; Wang, H. I.; Miyata, K.; Zhu, X.; Bonn, M. Quantifying Polaron Formation and Charge Carrier Cooling in Lead-Iodide Perovskites. *Adv. Mater.* **2018**, *30*, 1707312.

(12) Seiler, H.; Palato, S.; Sonnichsen, C.; Baker, H.; Socie, E.; Strandell, D. P.; Kambhampati, P. Two-Dimensional Electronic Spectroscopy Reveals Liquid-Like Lineshape Dynamics in CsPbI3 Perovskite Nanocrystals. *Nat. Commun.* **2019**, *10*, 4962.

(13) Wu, X.; Tan, L. Z.; Shen, X.; Hu, T.; Miyata, K.; Trinh, M. T.; Li, R.; Coffee, R.; Liu, S.; Egger, D. A.; Makasyuk, I.; Zheng, Q.; Fry, A.; Robinson, J. S.; Smith, M. D.; Guzelturk, B.; Karunadasa, H. I.; Wang, X.; Zhu, X.; Kronik, L.; Rappe, A. M.; Lindenberg, A. M. Light-Induced Picosecond Rotational Disordering of the Inorganic Sublattice in Hybrid Perovskites. *Science Advances* **2017**, *3*, e1602388.

(14) Guzelturk, B.; Winkler, T.; Van de Goor, T. W. J.; Smith, M. D.; Bourelle, S. A.; Feldmann, S.; Trigo, M.; Teitelbaum, S. W.; Steinruck, H.-G.; de la Pena, G. A.; Alonso-Mori, R.; Zhu, D.; Sato, T.; Karunadasa, H. I.; Toney, M. F.; Deschler, F.; Lindenberg, A. M. Visualization of Dynamic Polaronic Strain Fields in Hybrid Lead Halide Perovskites. *Nat. Mater.* **2021**, *20*, 618−623.

(15) Gebhardt, J.; Kim, Y.; Rappe, A. M. Influence of the Dimensionality and Organic Cation on Crystal and Electronic Structure of Organometallic Halide Perovskites. *J. Phys. Chem. C* **2017**, *121*, 6569−6574.

(16) Pedesseau, L.; Sapori, D.; Traore, B.; Robles, R.; Fang, H.-H.; Loi, M. A.; Tsai, H.; Nie, W.; Blancon, J.-C.; Neukirch, A.; Tretiak, S.; Mohite, A. D.; Katan, C.; Even, J.; Kepenekian, M. Advances and Promises of Layered Halide Hybrid Perovskite Semiconductors. *ACS Nano* **2016**, *10*, 9776−9786.

(17) Katan, C.; Mercier, N.; Even, J. Quantum and Dielectric Confinement Effects in Lower-Dimensional Hybrid Perovskite Semiconductors. *Chem. Rev.* **2019**, *119*, 3140−3192.

(18) Straus, D. B.; Kagan, C. R. Electrons, Excitons, and Phonons in Two-Dimensional Hybrid Perovskites: Connecting Structural, Optical, and Electronic Properties. *J. Phys. Chem. Lett.* **2018**, *9*, 1434−1447.

(19) Srimath Kandada, A. R.; Silva, C. Exciton Polarons in Two-Dimensional Hybrid Metal-Halide Perovskites. *J. Phys. Chem. Lett.* **2020**, *11*, 3173−3184.
(20) Zhang, H.; Li, W.; Essman, J.; Quarti, C.; Metcalf, I.; Chiang, W.-Y.; Sidhik, S.; Hou, J.; Fehr, A.; Attar, A.; Lin, M.-F.; Britz, A.; Shen, X.; Link, S.; Wang, X.; Bergmann, U.; Kanatzidis, M. G.; Katan, C.; Even, J.; Blancon, J.-C.; Mohite, A. D.Direct Visualization of Ultrafast Lattice Ordering Triggered by an Electron-Hole Plasma in 2D Perovskites. *arXiv (Condensed Matter Materials Science)*, Apr. 3, 2022, 2204.01145, ver. 1. https://arxiv.org/abs/2204.01145.
(21) Smith, M. D.; Karunadasa, H. I. White-Light Emission from Layered Halide Perovskites. *Acc. Chem. Res.* **2018**, *51*, 619−627.
(22) Ni, L.; Huynh, U.; Cheminal, A.; Thomas, T. H.; Shivanna, R.; Hinrichsen, T. F.; Ahmad, S.; Sadhanala, A.; Rao, A. Real-Time Observation of Exciton−Phonon Coupling Dynamics in Self-Assembled Hybrid Perovskite Quantum Wells. *ACS Nano* **2017**, *11*, 10834−10843.
(23) Straus, D. B.; Hurtado Parra, S.; Iotov, N.; Gebhardt, J.; Rappe, A. M.; Subotnik, J. E.; Kikkawa, J. M.; Kagan, C. R. Direct Observation of Electron-Phonon Coupling and Slow Vibrational Relaxation in Organic-Inorganic Hybrid Perovskites. *J. Am. Chem. Soc.* **2016**, *138*, 13798−13801.
(24) Neutzner, S.; Thouin, F.; Cortecchia, D.; Petrozza, A.; Silva, C.; Srimath Kandada, A. R. Exciton-Polaron Spectral Structures in Two-Dimensional Hybrid Lead-Halide Perovskites. *Physical Review Materials* **2018**, *2*, 064605.
(25) Straus, D. B.; Iotov, N.; Gau, M. R.; Zhao, Q.; Carroll, P. J.; Kagan, C. R. Longer Cations Increase Energetic Disorder in Excitonic 2D Hybrid Perovskites. *J. Phys. Chem. Lett.* **2019**, *10*, 1198−1205.
(26) Straus, D. B.; Hurtado Parra, S.; Iotov, N.; Zhao, Q.; Gau, M. R.; Carroll, P. J.; Kikkawa, J. M.; Kagan, C. R. Tailoring Hot Exciton Dynamics in 2D Hybrid Perovskites Through Cation Modification. *ACS Nano* **2020**, *14*, 3621−3629.
(27) Straus, D. B.; Kagan, C. R. Photophysics of Two-Dimensional Semiconducting Organic-Inorganic Metal-Halide Perovskites. *Annu. Rev. Phys. Chem.* **2022**, *73*, 403.
(28) Robinson, K.; Gibbs, G. V.; Ribbe, P. H. Quadratic Elongation: A Quantitative Measure of Distortion in Coordination Polyhedra. *Science* **1971**, *172*, 567−570.
(29) Yazdani, N.; Bodnarchuk, M. I.; Bertolotti, F.; Masciocchi, N.; Fureraj, I.; Guzelturk, B.; Cotts, B. L.; Zajac, M.; Rainò, G.; Jansen, M.; Boehme, S. C.; Yarema, M.; Lin, M.-F.; Kozina, M.; Reid, A.; Shen, X.; Weathersby, S.; Wang, X.; Vauthey, E.; Guagliardi, A.; Kovalenko, M. V.; Wood, V.; Lindenberg, A.Phonon-Mediated Attractive Interactions between Excitons in Lead-Halide-Perovskites. *arXiv (Condensed Matter Materials Science)*, Mar. 11, 2022, 2203.06286v1, ver. 1. https://arxiv.org/abs/2203.06286 (accessed March 25, 2022).
(30) Mao, L.; Wu, Y.; Stoumpos, C. C.; Wasielewski, M. R.; Kanatzidis, M. G. White-Light Emission and Structural Distortion in New Corrugated Two-Dimensional Lead Bromide Perovskites. *J. Am. Chem. Soc.* **2017**, *139*, 5210−5215.
(31) Cortecchia, D.; Neutzner, S.; Srimath Kandada, A. R.; Mosconi, E.; Meggiolaro, D.; De Angelis, F.; Soci, C.; Petrozza, A. Broadband Emission in Two-Dimensional Hybrid Perovskites: The Role of Structural Deformation. *J. Am. Chem. Soc.* **2017**, *139*, 39−42.
(32) Cortecchia, D.; Yin, J.; Bruno, A.; Lo, S.-Z. A.; Gurzadyan, G. G.; Mhaisalkar, S.; Brédas, J.-L.; Soci, C. Polaron Self-Localization in White-Light Emitting Hybrid Perovskites. *J. Mater. Chem. C* **2017**, *5*, 2771−2780.
(33) Hu, T.; Smith, M. D.; Dohner, E. R.; Sher, M.-J.; Wu, X.; Trinh, M. T.; Fisher, A.; Corbett, J.; Zhu, X.-Y.; Karunadasa, H. I.; Lindenberg, A. M. Mechanism for Broadband White-Light Emission from Two-Dimensional (110) Hybrid Perovskite. *J. Phys. Chem. Lett.* **2016**, *7*, 2258−2263.
(34) Smith, M. D.; Jaffe, A.; Dohner, E. R.; Lindenberg, A. M.; Karunadasa, H. I. Structural Origins of Broadband Emission From Layered Pb−Br Hybrid Perovskites. *Chemical Science* **2017**, *8*, 4497−4504.
(35) Baranowski, M.; Urban, J. M.; Zhang, N.; Surrente, A.; Maude, D. K.; Andaji-Garmaroudi, Z.; Stranks, S. D.; Plochocka, P. Static and Dynamic Disorder in Triple-Cation Hybrid Perovskites. *J. Phys. Chem. C* **2018**, *122*, 17473−17480.
(36) Wu, X.; Trinh, M. T.; Niesner, D.; Zhu, H.; Norman, Z.; Owen, J. S.; Yaffe, O.; Kudisch, B. J.; Zhu, X.-Y. Trap States in Lead Iodide Perovskites. *J. Am. Chem. Soc.* **2015**, *137*, 2089−2096.
(37) Price, M. B.; Butkus, J.; Jellicoe, T. C.; Sadhanala, A.; Briane, A.; Halpert, J. E.; Broch, K.; Hodgkiss, J. M.; Friend, R. H.; Deschler, F. Hot-Carrier Cooling and Photoinduced Refractive Index Changes in Organic−Inorganic Lead Halide Perovskites. *Nat. Commun.* **2015**, *6*, 8420.
(38) Yang, Y.; Ostrowski, D. P.; France, R. M.; Zhu, K.; van de Lagemaat, J.; Luther, J. M.; Beard, M. C. Observation of a Hot-Phonon Bottleneck in Lead-Iodide Perovskites. *Nat. Photonics* **2016**, *10*, 53.
(39) Trinh, M. T.; Wu, X.; Niesner, D.; Zhu, X.-Y. Many-Body Interactions in Photo-Excited Lead Iodide Perovskite. *Journal of Materials Chemistry A* **2015**, *3*, 9285−9290.
(40) Thouin, F.; Neutzner, S.; Cortecchia, D.; Dragomir, V. A.; Soci, C.; Salim, T.; Lam, Y. M.; Leonelli, R.; Petrozza, A.; Kandada, A. R. S.; Silva, C. Stable Biexcitons in Two-Dimensional Metal-Halide Perovskites With Strong Dynamic Lattice Disorder. *Physical Review Materials* **2018**, *2*, 034001.
(41) Wu, X.; Trinh, M. T.; Zhu, X. Y. Excitonic Many-Body Interactions in Two-Dimensional Lead Iodide Perovskite Quantum Wells. *J. Phys. Chem. C* **2015**, *119*, 14714−14721.
(42) Thouin, F.; Valverde-Chavez, D. A.; Quarti, C.; Cortecchia, D.; Bargigia, I.; Beljonne, D.; Petrozza, A.; Silva, C.; Srimath Kandada, A. R. Phonon Coherences Reveal the Polaronic Character of Excitons in Two-Dimensional Lead Halide Perovskites. *Nat. Mater.* **2019**, *18*, 349−356.
(43) Chatterjee, A. Strong-Coupling Theory for the Multidimensional Free Optical Polaron. *Phys. Rev. B* **1990**, *41*, 1668−1670.
(44) Chen, C. Y.; Lin, D. L.; Jin, P. W.; Zhang, S. Q.; Chen, R. Strong-Coupling Theory of Quasi-Two-Dimensional Polarons. *Phys. Rev. B* **1994**, *49*, 13680−13684.
(45) Peeters, F. M.; Xiaoguang, W.; Devreese, J. T. Ground-State Energy of a Polaron in N Dimensions. *Phys. Rev. B* **1986**, *33*, 3926−3934.
(46) Peeters, F. M.; Devreese, J. T. Scaling Relations Between the Two- and Three-Dimensional Polarons for Static and Dynamical Properties. *Phys. Rev. B* **1987**, *36*, 4442−4445.
(47) Devreese, J. T.; Alexandrov, A. S. Fröhlich Polaron and Bipolaron: Recent Developments. *Rep. Prog. Phys.* **2009**, *72*, 066501.
(48) Hong, X.; Ishihara, T.; Nurmikko, A. V. Dielectric Confinement Effect on Excitons in PbI_4-Based Layered Semiconductors. *Phys. Rev. B* **1992**, *45*, 6961−6964.
(49) Dohner, E. R.; Jaffe, A.; Bradshaw, L. R.; Karunadasa, H. I. Intrinsic White-Light Emission from Layered Hybrid Perovskites. *J. Am. Chem. Soc.* **2014**, *136*, 13154−13157.
(50) Emin, D.; Holstein, T. Adiabatic Theory of an Electron in a Deformable Continuum. *Phys. Rev. Lett.* **1976**, *36*, 323−326.
(51) Harris, J. H.; Nurmikko, A. V. Formation of the Bound Magnetic Polaron in (Cd,Mn)Se. *Phys. Rev. Lett.* **1983**, *51*, 1472−1475.

https://doi.org/10.1021/acsnano.2c09256
ACS Nano 2022, 16, 21259−21265